Available online at www.sciencedirect.com
ScienceDirect
Acta Materialia 56 (2008) 2570–2575
Acta MATERIALIA
www.elsevier.com/locate/actamat

Experimental examination of displacement and strain fields in an edge dislocation core

C.W. Zhao [a,*], Y.M. Xing [a], C.E. Zhou [a], P.C. Bai [b]

[a] College of Science, Inner Mongolia University of Technology, 010051 Hohhot, China
[b] College of Materials Science and Engineering, Inner Mongolia University of Technology, 010051 Hohhot, China

Received 19 December 2007; received in revised form 22 January 2008; accepted 26 January 2008
Available online 6 March 2008

Abstract

We present a displacement and strain analysis of edge dislocation core in gold. The displacement and strain field around the edge dislocation were mapped by geometric phase analysis of high-resolution transmission electron microscopy images. The displacement and strain measurement results were compared with the isotropic elastic theory dislocation model, the anisotropic elastic theory dislocation model, the Peierls–Nabarro dislocation model and the Foreman dislocation model ($a = 4$). These comparisons show that the Peierls–Nabarro model is the most appropriate theoretical model to describe the deformation fields of the dislocation core.

Keywords: Dislocations; Displacement; Strain; High-resolution electron microscopy; Geometric phase analysis

1. Introduction

Dislocation plays a very important role in a material's mechanical properties. Research on dislocations is a classical topic in materials science and attracts a lot of scientific interest. There are many dislocation models, such as the elastic theory model and discrete model. The Peierls–Nabarro [1–3] dislocation model is one of the most important models and has been discussed by many researchers [4–6]. Foreman proposed an improved model [7]. In this model, the Peierls–Nabarro dislocation model is extended to a family of edge dislocations of greater widths by introducing the factor a. Foreman thought that $a = 4$ was fitted for bubble raft experiments.

The core structure of an edge dislocation in gold has been studied using a molecular dynamics simulation [8]. The dislocation core properties of the Peierls–Nabarro model were also theoretically studied by Lu [9] and Schoeck [10]. Although a lot of research has already been done in this field, there are still many problems that remain unsolved. For example, a direct measurement to verify the Peierls–Nabarro model has not been achieved because of a lack of experimental techniques with sufficient displacement sensitivity and spatial resolution. Recently, high-resolution transmission electron microscopy (HRTEM) has become a powerful tool for mapping the displacement field at the nanoscale level because of the development of quantitative image analysis methods [11–12]. One such technique is geometric phase analysis (GPA) [13], which has been applied to a wide variety of systems, such as quantum dots [14], nanowires [15], Si/Ge heterostructures [16] and low-angle grain boundaries [17]. The GPA has also been applied to quantitative measurements of displacement fields of edge dislocation in aluminum [18]. The accuracy of the technique has demonstrated that could be measured to 0.003 nm [19]. Here, we present a study of an edge dislocation in gold. The displacement fields and strain fields of the dislocation core were mapped and compared with four dislocation models.

* Corresponding author.
E-mail address: zhaocw@imut.edu.cn (C.W. Zhao).

1359-6454/$34.00
doi:10.1016/j.actamat.2008.01.045

2. Theory

2.1. Displacement of edge dislocation given by isotropic elastic theory

The isotropic elastic theory describes the displacement of an edge dislocation as

$$u_x = \frac{b}{2\pi}\left[\tan^{-1}\frac{y}{x} + \frac{xy}{2(1-v)(x^2+y^2)}\right] \tag{1}$$

$$u_y = -\frac{b}{2\pi}\left[\frac{1-2v}{4(1-v)}\ln(x^2+y^2) + \frac{x^2-y^2}{4(1-v)(x^2+y^2)}\right] \tag{2}$$

where x and y are the right-angle coordinates, respectively, centered on the dislocation core position, b is the Burgers vector, and v the Poisson ratio.

2.2. Displacement of edge dislocation given by anisotropic elastic theory

The anisotropic elastic theory describes the displacement of an edge dislocation $b = (b_x, b_y, 0)$ as

$$\begin{aligned} u_x = {} & -\frac{b_x}{4\pi}\left(\tan^{-1}\frac{2xy\lambda\sin\phi}{x^2-\lambda^2y^2} + \frac{\overline{c}'^2_{11}-c'^2_{12}}{2\overline{c}'_{11}c'_{66}\sin 2\phi}\ln\frac{q}{t}\right) \\ & - \frac{b_y}{4\pi\lambda\overline{c}'_{11}\sin 2\phi}\left[(\overline{c}'_{11}-c'_{12})\cos\phi\ln qt\right. \\ & \left. - \left(\overline{c}'_{11}+c'_{12}\right)\sin\phi\tan^{-1}\frac{x^2\sin 2\phi}{\lambda^2y^2-x^2\cos 2\phi}\right] \end{aligned} \tag{3}$$

$$\begin{aligned} u_y = {} & \frac{\lambda b_x}{4\pi\overline{c}'_{11}\sin 2\phi}\left[(\overline{c}'_{11}-c'_{12})\cos\phi\ln qt - (\overline{c}'_{11}+c'_{12})\right. \\ & \left.\times\sin\phi\tan^{-1}\frac{y^2\lambda^2\sin 2\phi}{x^2-\lambda^2y^2\cos 2\phi}\right] \\ & - \frac{b_y}{4\pi}\left(\tan^{-1}\frac{2xy\lambda\sin\phi}{x^2-\lambda^2y^2} - \frac{\overline{c}'^2_{11}-c'^2_{12}}{2\overline{c}'_{11}c'_{66}\sin 2\phi}\ln\frac{q}{t}\right) \end{aligned} \tag{4}$$

where $\phi = \frac{1}{2}\cos^{-1}\left(\frac{c'^2_{12}+2c'_{12}c'_{66}-\overline{c}'^2_{11}}{2\overline{c}'_{11}c'_{66}}\right)$, $\lambda = \left(\frac{c'_{11}}{c'_{12}}\right)^{\frac{1}{4}}$, $\overline{c}'_{11} = (c'_{11}c'_{12})^{1/2}$, $q^2 = x^2 + 2xy\lambda\cos\phi + y^2\lambda^2$ and $t^2 = x^2 - 2xy\lambda\cos\phi + y^2\lambda^2$. The $c'_{11}, c'_{12}, c'_{22}, c'_{66}$ are elastic constants.

2.3. Displacement of edge dislocation given by the Peierls–Nabarro model

According to the Peierls–Nabarro dislocation model, the displacement of an edge dislocation along the x direction can be written as

$$u_x = -\frac{b}{2\pi}\tan^{-1}\frac{2(1-v)x}{y} \tag{5}$$

2.4. Displacement of edge dislocation given by the Foreman model

Foreman has given a dislocation model, which describes the displacement of an edge dislocation along x direction as

$$u_x = -\frac{b}{2\pi}\left[\tan^{-1}\frac{2(1-v)x}{ay} + (a-1)\frac{2(1-v)xy}{4(1-v)^2x^2+a^2y^2}\right] \tag{6}$$

where a is an alterable parameter controlling dislocation width. Foreman thought that $a = 4$ was fitted for the bubble raft dislocation. It would be the Peierls–Nabarro model when $a = 1$.

3. Experimental methods

3.1. Geometric phase analysis

An HRTEM image formed at a zone axis of a crystal can be considered as a set of interference fringes corresponding to the atomic planes of the specimen. GPA analyzes these interference fringes individually to extract the information concerning displacement. In particular, the technique measures the displacement of lattice fringes with respect to a perfect lattice (for example provided by a region of undistorted substrate). The method is based on the calculation the local Fourier components of lattice fringes. The phase of these local Fourier components, or geometric phase $P_g(\boldsymbol{r})$, is directly related to the component of the displacement field, $\boldsymbol{u}(\boldsymbol{r})$, in the direction of the reciprocal lattice vector $\boldsymbol{g}$:

$$P_g(\boldsymbol{r}) = -2\pi\boldsymbol{g}\cdot\boldsymbol{u}(\boldsymbol{r}) \tag{7}$$

It is assumed that the displacement field is constant along the propagation direction through the foil or that if there are small variations, they are averaged out. In the latter case, the displacement field is the projected displacement field averaged over the foil thickness. And by measuring two phase images, $P_{g1}(\boldsymbol{r})$ and $P_{g2}(\boldsymbol{r})$, the two-dimensional displacement field can be determined:

$$\boldsymbol{u}(\boldsymbol{r}) = -\frac{1}{2\pi}[P_{g1}(\boldsymbol{r})\boldsymbol{a}_1 + P_{g2}(\boldsymbol{r})\boldsymbol{a}_2] \tag{8}$$

Here $\boldsymbol{a}_1$ and $\boldsymbol{a}_2$ are the basis vectors for the lattice in real space corresponding to the reciprocal lattice defined by $\boldsymbol{g}_1$ and $\boldsymbol{g}_2$. Eq. (6) in matrix form is

$$\begin{pmatrix} u_x \\ u_y \end{pmatrix} = -\frac{1}{2\pi}\begin{pmatrix} a_{1x} & a_{2x} \\ a_{1y} & a_{2y} \end{pmatrix}\begin{pmatrix} P_{g1} \\ P_{g2} \end{pmatrix} \tag{9}$$

Plane strain can be written as

$$\begin{cases} \varepsilon_{xx} = \frac{\partial u_x}{\partial x} \\ \varepsilon_{yy} = \frac{\partial u_y}{\partial y} \\ \varepsilon_{xy} = \frac{1}{2}\left(\frac{\partial u_x}{\partial y} + \frac{\partial u_y}{\partial x}\right) \end{cases} \tag{10}$$

3.2. Electron microscopy

The HRTEM sample is a gold crystal specimen that consists of an ultra-thin layer of gold grown epitaxially into a single crystal along the [0 0 1] direction. HRTEM experi-

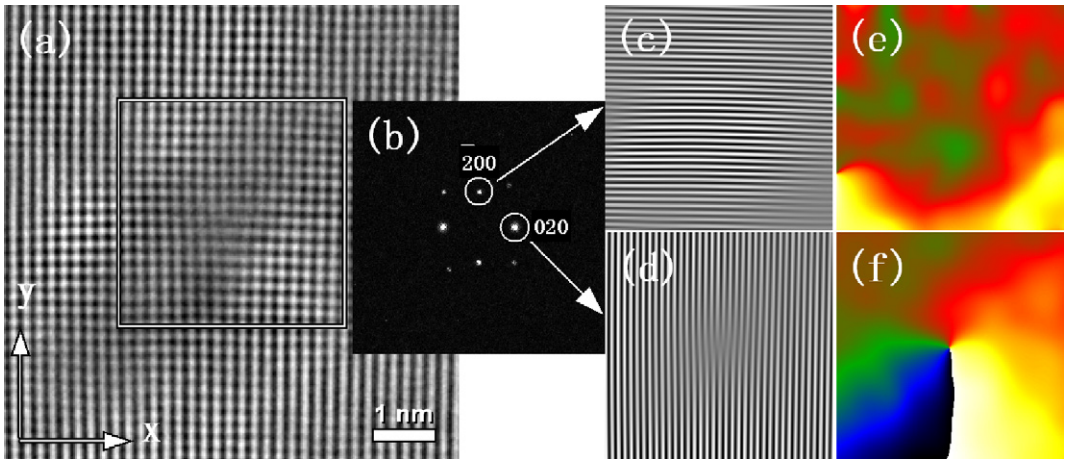

Fig. 1. Geometric phase analysis of an edge dislocation in a gold: (a) HRTEM image in [001] orientation; (b) Fourier transform of image in (a), with the analyzed spot circled; (c) $(\bar{2}00)$ lattice fringes obtained by filtering; (d) (020) lattice fringes obtained by filtering; (e) geometric phase image of $(\bar{2}00)$ lattice fringes and (f) geometric phase image of (020) lattice fringes. Color range $-\pi$ to π rad. (For interpretation of the references to color in this figure legend, the reader is referred to the web version of this article.)

ment was performed on the JEM-2010 transmission electron microscope at 200 kV (spherical aberration = 1.0 mm, point resolution = 0.194 nm). Images were recorded on a Gatan 1 k × 1 k slow scan CCD camera and processed using the software GPA Phase, developed by the Gatan DigitalMicrograph environment.

4. Results and discussion

Fig. 1a shows an HRTEM image of an edge dislocation in gold. Geometric phase images were calculated for the two sets of {200} lattice fringes (Fig. 1c and d) using Gaussian masks and are shown in Fig. 1e and f. Burgers vector $\boldsymbol{b} = 1/2[010]$. Taking the x-axis parallel to [010] and the y-axis parallel to $[\bar{1}00]$, the displacement field u_x can be calculated from geometric phase images and is shown in Fig. 2a. Also shown in Fig. 2 is the displacement field of four theoretical dislocation models that were calculated in an infinite medium using the bulk elastic constants of gold, $c'_{11} = c'_{22} = 186.0$ GPa, $c'_{12} = 157.0$ GPa, $c'_{66} = 42.0$ GPa, Poisson's ratio $v = 0.412$, lattice constant $a = 0.408$ nm. The color[1] scale indicates displacement changes of −0.051 nm to +0.051 nm. The displacement distribution of the experiment and the four theoretical models agree with each other in the region far from the dislocation core and have the asymptotic value of $u_x = \pm\frac{d_{020}}{4}$. Here, $u_x = \pm 0.051$ nm. Therefore, the isotropic elastic theory dislocation model, the anisotropic elastic theory dislocation model, the Peierls–Nabarro dislocation model and the Foreman dislocation model are all available far from dislocation core.

In order to quantitatively examine the degree of agreement between the experiment result and the four theoretical models in the region of the dislocation core, it is useful to consider the strain fields. Strain is particularly sensitive to noise, as it is calculated from the derivative of the displacement. The deformation fields are calculated for the boxed regions in Fig. 1a. The size of the boxed region is 3.725 nm × 3.725 nm. The strain field can be determined by numerically differentiating the displacement field. Therefore, the experimental strain field can be mapped and is shown in Fig. 3a. There is a convergence region of strain around the edge dislocation core. In the region of the extra half-plane ($y > 0$), the strains are negative and compressive, and the lattice is expanding on the other side. The largest strain values occur in the immediate core region. The strain is smaller farther from the dislocation core. Also shown in Fig. 3b–e are four theoretical model ε_{xx} strain fields. The color[1] scale indicates strain changes of –15% to +15%.

There is not a lot of obvious agreement in the vicinity of the dislocation core. The strain maps of isotropic elastic theory and anisotropic elastic theory are butterfly shape. The strain maps of the Peierls–Nabarro and the Foreman models are figure-of-eight-shaped. Thus, the four theoretical models are not all appropriate in the vicinity of the dislocation core. Qualitatively, the agreement of the experimental result and the Peierls–Nabarro dislocation model is in the best agreement. Also, we find that the elastic theory dislocation models are inappropriate theoretical models for the dislocation core.

To analyze the degree of agreement between the experiment and theory in more detail, we have selected four different circles of radius r from the dislocation core to measure the variation of strain and compared them with four theoretical models (the measurement location; see Fig. 3e). The results are shown in Fig. 4a–d. The standard deviations of the strain difference between the experimental and theoretical ε_{xx} strain components for different circle of radius r are shown in Table 1. The difference between the

[1] For interpretation of color in Figs. 2 and 3, the reader is referred to the web version of this article.

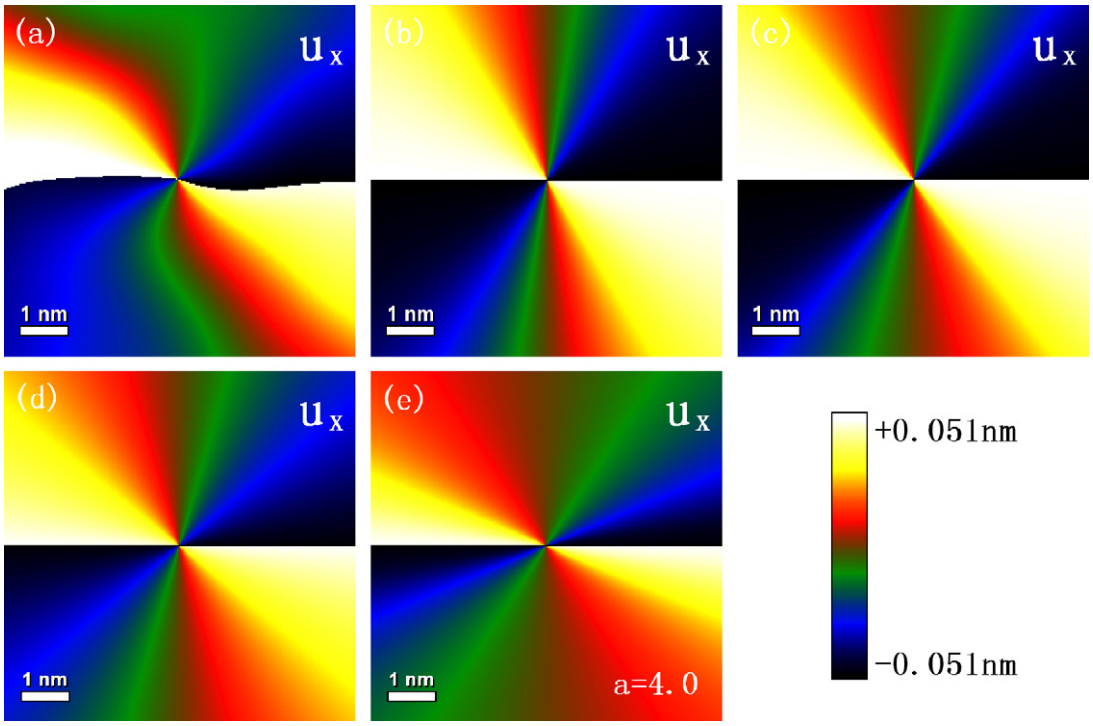

Fig. 2. Experimental and theoretical displacement fields: (a) experimental u_x displacement field; (b) isotropic elastic theory u_x displacement field; (c) anisotropic elastic theory u_x displacement field; (d) Peierls–Nabarro dislocation model u_x displacement field and (e) Foreman dislocation model ($a = 4.0$) u_x displacement field.

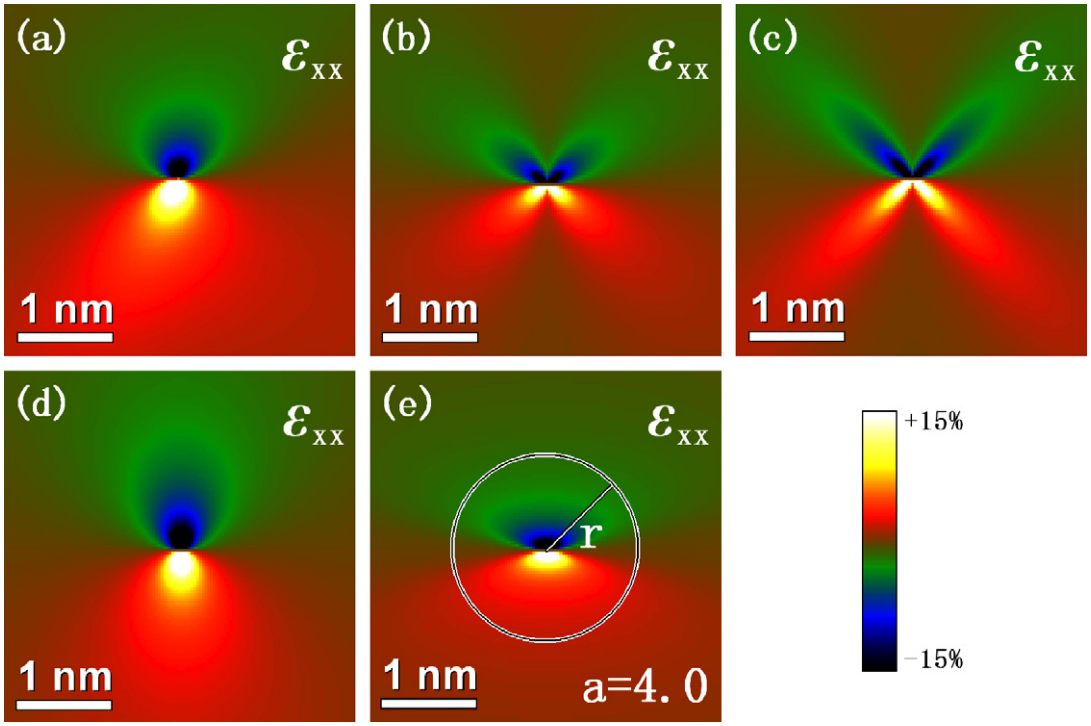

Fig. 3. Experimental and theoretical strain field: (a) experimental ε_{xx} strain field; (b) isotropic elastic theory ε_{xx} strain field; (c) anisotropic elastic theory ε_{xx} strain field; (d) Peierls–Nabarro dislocation model ε_{xx} strain field and (e) Foreman dislocation model ($a = 4.0$) ε_{xx} strain field.

experimental and the Peierls–Nabarro dislocation model ε_{xx} strain component is the smallest, while the difference between the experimental and anisotropic elastic theory ε_{xx} strain component is the greatest. Again, the agreement of the experimental result and the Peierls–Nabarro dislocation model is best.

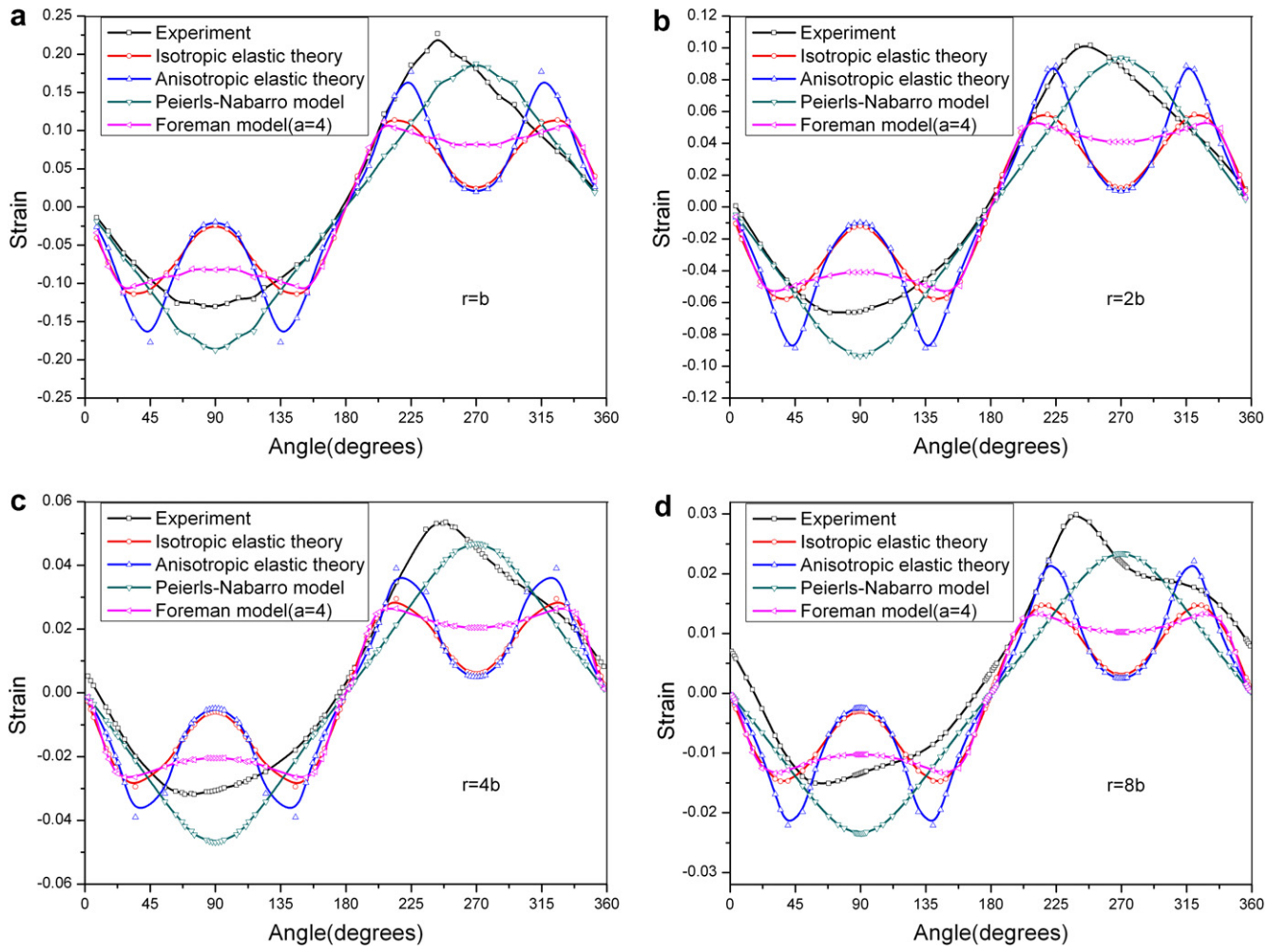

Fig. 4. Comparison of angular variation of strain field: (a) $r = b$; (b) $r = 2b$; (c) $r = 4b$ and (d) $r = 8b$.

Table 1
Standard deviations on the differences between the experimental and theoretical ε_{xx} strain components

	$r = b$	$r = 2b$	$r = 4b$	$r = 8b$
Experiment and isotropic elastic theory	0.075	0.036	0.020	0.0093
Experiment and anisotropic elastic theory	0.079	0.039	0.020	0.0096
Experiment and Peierls–Nabarro model	0.029	0.012	0.0061	0.0040
Experiment and Foreman model	0.053	0.024	0.013	0.0059

5. Conclusions

A direct quantitative measurement of the displacement and strain field around an edge dislocation core in gold was achieved by a combination of HRTEM and GPA. The displacement measurement region is 7.45×7.45 nm. The strain measurement region is 3.725×3.725 nm. The isotropic elastic theory dislocation model, the anisotropic elastic theory dislocation model, the Peierls–Nabarro dislocation model and the Foreman dislocation model ($a = 4$) are all appropriate far from the dislocation core (>7.5 nm). According to the comparison results of four theoretical models and the experimental results in the vicinity of the dislocation core, the Peierls–Nabarro model is the most appropriate theoretical model to describe the displacement field and strain field of the dislocation core in gold.

Acknowledgements

This work was supported by the National Natural Science Foundation of China Nos. 10562003 and 10272054. This work was also supported by the College Science Research Project in Inner Mongolia Autonomous Region No. NJ06062 and the Key Research Project in Inner Mongolia University of Technology No. ZD200710.

References

[1] Hirth JP, Lothe J. Theory of dislocation. New York: Wiley; 1982.
[2] Peierls RE. Proc Phys Soc London 1940;52:34.
[3] Nabarro FRN. Proc Phys Soc London 1947;59:256.

[4] Ren Q, Joós B, Duesbery MS. Phys Rev B 1995;52:13223.
[5] Hansen LB, Stokbro K, Lundqvist BI, Jacobsen KW, Deaven DM. Phys Rev Lett 1995;75:4444.
[6] Wang SF. Phys Rev B 2002;65:094111.
[7] Foreman AJ, Jaswon MA, Wood JK. Proc Phys Soc London A 1951;64:156.
[8] Wang R, Fang QF. J Alloy Comp 2000;310:80.
[9] Lu G, Kioussis N, Bulatov VV, Kaxiras E. Mater Sci Eng A 2001;309–310:142.
[10] Schoeck G. Acta Mater 2001;49:1179.
[11] Kret S, Ruterana P, Rosenauer A, Gerthsen D. Phys Status Solidi B 2001;227:247.
[12] Ang KW, Chui KJ, Bliznetsov V, Tung CH, Du A, Balasubramanian N, et al. Appl Phys Lett 2005;86:093102.
[13] Hÿtch MJ, Snoeck E, Kilaas R. Ultramicroscopy 1998;74:131.
[14] Sarigiannidou E, Monroy E, Daudin B, Rouvière JL, Andreev AD. Appl Phys Lett 2005;87:203112.
[15] Taraci JL, Hÿtch MJ, Clement T, Peralta P, McCartney MR, Jeff Drucker, et al. Nanotechnology 2005;16:2365.
[16] Hÿtch MJ, Houdellier F. Microelectron Eng 2007;84:460.
[17] Zhao CW, Xing YM, Bai PC, Hou JF, Dai XJ. Physica B 2008;403:1838.
[18] Zhao CW, Xing YM, Bai PC. Phys Lett A 2008;372:312.
[19] Hÿtch MJ, Putaux J-L, Pénisson J-M. Nature 2003;423:270.